

Thermal Modeling and Experimental Validation of Mid-Conductor Winding Cooling

Ilya T’Jollyn^{a,b*}, Jasper Nonneman^{a,b} and Michel De Paepe^{a,b}

^aDepartment of Electromechanical, Systems and Metal Engineering, Ghent University, Ghent, Belgium; ^bFlandersMake@UGent – Core lab EEDT-MP, Leuven, Belgium

*Sint-Pietersnieuwstraat 41, Ghent, 9000, Belgium, e-mail: ilya.tjollyn@ugent.be, tel.: +3292643250

ORCiDs:

Ilya T’Jollyn: 0000-0003-3151-260X

Jasper Nonneman: 0000-0001-6196-3757

Michel De Paepe: 0000-0003-0233-0719

Thermal Modeling and Experimental Validation of Mid-Conductor Winding Cooling

A direct cooling method for windings of electrical machines, mid-conductor winding cooling, is studied. Spaces between the wires are utilized as coolant channels, with a liquid being pumped through the winding along the length. This results in the elimination of thermal interface resistances, a high heat transfer area and heat transfer coefficient while maintaining the same cross-sectional area for the copper winding. A thermohydraulic model is made and validated to analyze the heat transfer rates and pressure drop. Validation measurements with a water-glycol mixture as coolant show that the modeled and measured pressure drop correspond within 0.07 bar and the modeled and measured winding temperature within 3 °C. When made relative to the temperature difference between winding and coolant, the deviation is equal to 12%. The validated model is used to analyze the performance when utilizing oil as coolant. For a winding temperature of 180 °C and a pressure drop of 1 bar, using the novel cooling method results in a maximal attainable current density equal to 39.4 A/mm² which is 41% higher than that attainable with spray end winding cooling.

Keywords: electric machine, windings, heat transfer, thermal management, direct oil cooling, mid-conductor winding cooling

Introduction

To reduce the emissions of the transport sector, electrification of vehicles is considered as one of the main solutions. With the increase in production of electric vehicles comes a drive for electric motors with higher power density [1]. An electric motor with a higher power density but similar power will be lighter, thereby increasing the vehicle driving range, at a potentially lower cost. Improvements in power density can be made on several aspects, such as mechanical and magnetic characteristics. However, the thermal behavior (and thus cooling) of the electric machine is typically one of the main bottlenecks [2]–[4]. For many applications, the power output of the machine is limited by the maximal temperature in the windings, which is restricted by the winding

insulation material which degrades at too high temperatures [5]. There are two main causes for the difficulty of cooling windings in traditional machines: the low thermal conductivity perpendicular to the direction of the wires and the thermal interface resistances at the interfaces between dissimilar materials in the machine [6].

Many techniques to reduce or remove these thermal resistance have been proposed in scientific literature [7]. Liquid cooling is being used in nearly all traction electric machines, as it outperforms air cooling methods [7]. This is typically implemented through a water jacket which provides cooling at the outer diameter of the machine. A possibility to reduce the total thermal resistance is adding a highly conductive path from the winding to the liquid cooling jacket. For example, adding copper bars [8] or heat pipes [9] through the stator iron results in improved cooling. A similar method can be applied in the end space, by adding inserts which create an additional conductive heat transfer path from end winding to water jacket [10]. Although these methods provide significant improvements, the thermal performance is still hampered by thermal contact resistances and the low effective thermal conductivity of the winding. Many studies propose bringing the coolant closer to the windings to remove interface resistances. Additional liquid cooling can be added at the end windings, for example by adding coolant channels [11], by spraying or impinging fluids [12], [13] or by pool boiling with fluorocarbons [14]. Although cooling at the end windings removes several thermal interface resistances, the available additional surface area for cooling is a rather small part of the entire winding. An alternative to end winding cooling is to cool the active part of the winding, by having the coolant flow axially through the machine. This can be implemented in the stator slots, by adding tubes [15] or by direct contact with the winding [16]. A more advanced method is to integrate coolant conduits within Litz wires which make up the winding [17]. The main

drawback of these methods is the reduction in volume available for copper in the stator slots. Another option for improved winding cooling is by using 3D printed or casted coils which are form integrated cooling channels [18]. This allows for direct contact between coolant and winding and can have a large cooling surface due to the multitude of channels, while still having a large volume in the slot used as conductors for the winding. The disadvantage of this method is that it requires a non-standard and expensive winding technology. To summarize, all these methods significantly improve the cooling performance. However, they are all hampered by one or more of the following disadvantages: thermal interface resistances, small heat transfer areas, reduced conductor volume or non-standard winding techniques.

As all the described techniques were applied to various kinds and sizes of motors, it is not straight-forward to compare the different techniques. A useful parameter is the current density of the winding, which is defined as the current through the conductors divided by the cross-sectional area of the conductors. The higher this value, the better the winding must be cooled to operate below the temperature limit of the insulation. The maximal current density is then reached when the maximal temperature in the winding is attained. This value is also dependent on the boundary conditions used, such as the coolant inlet temperature, wire insulation class, winding fill factor and axial length of the motor. If the coolant inlet temperature is lower or if the wire insulation class allows for higher winding temperatures, higher current densities can be achieved for an identical cooling technique. A winding with a lower fill factor will be able to reach higher current densities with identical cooling, as less heat will be generated. Motors with a longer axial length will be able to handle lower current densities with the same kind of end winding cooling. Although all these parameters besides the cooling technique also influence the current density, they do not vary greatly

for the electric machines under consideration in this analysis. It is thus fair to say that acquiring a higher current density relates to a better cooling system.

Table 1 shows some current density values for common cooling techniques, gathered from [19], as well as current densities for several advanced cooling techniques described here. From the data available in these references, the boundary conditions as mentioned in the previous section are rather similar (maximal temperature difference between winding and coolant ranges from 115 °C to 160 °C, the winding fill factor from 45% to 49% and the active axial length from 80 mm to 130 mm). With liquid cooling higher current densities can be achieved than with air cooling. Furthermore, the current densities for the advanced liquid cooled techniques all fall within the range 10-30 A/mm², with the casted coil as outlier at 100 A/mm². The major disadvantage of the latter technique is that it requires a non-standard and expensive winding technology. In this paper, a cooling method is proposed which uses the standard winding technologies but achieves a similar cooling technique and has an improved thermal performance compared to other cooling techniques on standard windings.

The goal of this study is to describe, model and test this new cooling method and thereby analyze its potential to enhance the cooling of electric machines. The following section explains in detail the cooling technique. Next, a thermohydraulic model of the cooling method is developed and the performed validation measurements and thermal performance with water-glycol as coolant are described. Finally, the prospective performance with oil as coolant is illustrated with the validated model.

Mid-conductor winding cooling

The novel winding cooling method described in this paper is coined ‘Mid-conductor winding cooling’ (MCWC). This method utilizes the free space in between the

individual wires as coolant channels. This free space is inevitably present, but is usually filled with an impregnation or potting material. The coolant is contained by a housing around the winding, which also provides the mechanical support for the winding. The flow path of the coolant starts at one end of the motor, splits and flows along the multiple strands of the winding, to eventually merge and exit at the other side of the motor (see Figure 1 for an example for a concentrated winding). A similar method has been found in US patent 6787948 B2, where the free spaces in between conductors in Litz wires are used as coolant channels [20].

The advantages of the proposed method are multiple. Firstly, all thermal interface resistances are eliminated as the coolant is in direct contact with the winding. The thermal resistance of the heat transfer through the winding itself is also eliminated by cooling inside the winding. Secondly, no reduction of copper area is needed as the coolant will only take up space which was not utilized in a winding without direct winding cooling. Another advantage is that due to the contact of every individual wire with the coolant, the heat transfer area is drastically increased when compared to cooling the outside surface of the winding, up to 50 times and more. Finally, due to the small hydraulic diameter of the channels formed in the winding, the heat transfer coefficient will be increased when compared to regular sized channels, i.e. microchannel heat transfer. The key novelty of the method is the combination of the direct through-slot winding cooling of all individual wires with the use of standard winding technologies.

Mid-conductor winding cooling can be used for distributed as well as concentrated winding types. A conceptual design for the cooling of concentrated stator windings is shown in Figure 2. It shows a six-pole stator with concentrated windings.

Each winding is equipped with a housing having an inlet and outlet to provide coolant flow in between the individual wires.

In conventional motors, windings are impregnated to fill the gaps in between the wires. This cannot be done for this cooling method, as the coolant needs to flow through these gaps. This poses some additional challenges, as the impregnation has multiple purposes. It improves heat conduction through the winding, serves as additional electrical insulation, provides mechanical strength and dampens vibrations.

Improvement of heat conduction is not necessary in this method, as the coolant is in direct contact with the wires. To ensure proper electrical insulation, a dielectric fluid should be used as coolant. The mechanical strength of the winding must be provided by the housing. The outer surface of the winding can be varnished to adhere to the housing for additional strength. Vibrations of the wires can be dampened by the fluid in contact with the individual wires. Although these challenges are of interest for further research, they are not further elaborated on here, as the focus of this paper is on the thermohydraulic feasibility of the cooling method.

Thermohydraulic model

The initial version of the thermohydraulic model was first described by the authors in a previous paper [21]. The equations governing the model are repeated here, as several improvements were made and it is validated with measurements in the following section.

To evaluate the proposed winding cooling method, the temperature of the winding must be determined. First the thermal resistance from the conductor to the cooling fluid is determined. The effect of the temperature rise of the coolant in the flow direction on the conductor temperature is also discussed. The pressure drop is estimated

as a function of the flow rate through the winding. When limiting the pressure drop to a set value, the winding temperature can be determined as a function of the winding heat dissipation.

Thermal resistance

To estimate the temperatures in the copper winding, a lumped parameter model is made for the heat transfer from the winding to the cooling fluid. It is assumed that the copper losses result in a uniform volumetric heat dissipation in the conductors. With the assumption of a two-dimensional temperature profile (infinitely long conductor) and axisymmetric cooling, the temperature profile T in the conductor can be described as a function of the distance from the centerline r as in Eq. (1).

$$T(r) = T_b + \frac{\dot{Q}_c}{4 \pi k_c L_{tot}} \left[1 - \left(\frac{2r}{D_c} \right)^2 \right] \quad (1)$$

In Eq. (1), T_b is the temperature at the boundary, \dot{Q}_c is the conductor heat dissipation, k_c is the conductor thermal conductivity, L_{tot} is the total wire length and D_c is the diameter of the conductor. The equivalent thermal resistance in the conductor R_c (between the centerline and boundary temperature for uniform volumetric heat dissipation) is given by Eq. (2).

$$R_c = \frac{T(0) - T_b}{\dot{Q}_c} = \frac{1}{4 \pi k_c L_{tot}} \quad (2)$$

An equivalent resistance for the insulation R_i can be defined as in Eq. (3).

$$R_i = \frac{\ln\left(\frac{D_i}{D_c}\right)}{2 \pi k_i L_{tot}} \quad (3)$$

Where D_i is the outer diameter of the wire with insulation and k_i is the insulation thermal conductivity.

For the convective thermal resistance, the flow is assumed to be laminar, since the channels are very small. This assumption will be checked and confirmed in the processing of the simulation results in model validation section. Although the heat dissipation in the conductors is nearly uniform (assuming the temperature variation and the resulting variation in electrical resistance is small), a constant temperature boundary condition for convective heat transfer is used in the modeling. Since the thermal resistance in the direction of the wire is very low compared to that perpendicular to the direction of the wire, temperatures along the length of the wire will be nearly constant. A constant temperature boundary is thus the best approximation for the heat transfer problem. The heat transfer in fully developed laminar flow is characterized by a constant Nusselt number, independent of any flow parameters. Estimations of the thermal development length indicate that the flow is not fully developed during the entire flow length, which would result in higher Nusselt numbers and heat transfer coefficients. Using the fully developed Nusselt number will therefore result in an overestimation of the winding temperature, making it a safe assumption. For perfect cylindrical packing, as in Figure 3 on the left, the flow channels are cusped channels with three sides, for which the Nusselt number Nu for a constant temperature boundary is equal to 0.916 [22]. From the Nusselt number, the thermal resistance of convection in the fluid R_f can be determined as in Eq. (4).

$$R_f = \frac{1}{h A} = \frac{D_h}{k_f Nu A} \quad (4)$$

With h the convective heat transfer coefficient, A the total surface area in contact with the fluid, D_h the hydraulic diameter of the channel and k_f the fluid thermal conductivity. For a perfect packing, the surface area $A_{perfect}$ is given by Eq. (5).

$$A_{perfect} = \pi D_i L_{tot} \quad (5)$$

If deformation occurs, part of the outer surface will be in contact with the neighboring wire and not the entire surface is in contact with the fluid. This effect can be included by adding a parameter ϵ , which ranges between 0 and 1, to determine the actual surface area as in Eq. (6). Figure 3 show two sets of packed wires: one without deformation on the left ($\epsilon = 0$) and one with deformation on the right ($\epsilon = 0.5$). This figure clearly shows the reduced contact area between coolant and wire for the deformed wires.

$$A = (1 - \epsilon)A_{perfect} \quad (6)$$

The hydraulic diameter is given by Eq. (7).

$$D_h = \frac{4S}{P} \quad (7)$$

In Eq. (7), S is the cross-sectional channel area and P is the perimeter. With some manipulations, the hydraulic diameter can be determined as in Eq. (8).

$$D_h = \left[\frac{1}{FF (D_c/D_i)^2} - 1 \right] \frac{D_i}{1-\epsilon} \quad (8)$$

With FF the fill factor of the winding, which is defined here as the ratio of the volume taken up by the conductor to the total volume of the winding (conductor, insulation and, in this case, fluid volume). The thermal resistance of convection can then be determined by Eq. (9).

$$R_f = \frac{\frac{1}{FF (D_c/D_i)^2} - 1}{\pi (1-\epsilon)^2 k_f Nu L_{tot}} \quad (9)$$

Temperature rise of the coolant

Next to the temperature differences due to heat transfer which can be calculated from the thermal resistances, the heating of the coolant along the length of the flow path will

have an influence on the temperature of the winding. As discussed in the previous section, a constant temperature boundary condition is assumed, which results in Eq. (10).

$$\dot{Q}_c = \frac{LMTD}{R_{tot}} = \frac{T_{f,o} - T_{f,i}}{\ln\left(\frac{T_c - T_{f,i}}{T_c - T_{f,o}}\right) R_{tot}} \quad (10)$$

With $LMTD$ the logarithmic mean temperature difference, R_{tot} the total thermal resistance equal to the sum of the conductor, insulation and convective thermal resistance and $T_{f,o}$ and $T_{f,i}$ respectively the outlet and inlet coolant temperature. The temperature difference between inlet and outlet temperature of the cooling fluid is determined by Eq. (11).

$$T_{f,o} - T_{f,i} = \frac{\dot{Q}_c}{\rho \dot{V} c_p} \quad (11)$$

In Eq. (11), ρ is the density of the fluid, \dot{V} is the volumetric flow rate and c_p is the specific heat capacity of the fluid. Combining Eq. (10) and Eq. (11) results in Eq. (12).

$$R_{tot} \rho \dot{V} c_p = \left[\ln \left(\left(1 - \frac{\dot{Q}_c}{\rho \dot{V} c_p (T_c - T_{f,i})} \right)^{-1} \right) \right]^{-1} \quad (12)$$

Rewriting Eq. (12) leads to Eq. (13).

$$T_c = T_{f,i} + \frac{\dot{Q}_c}{\rho \dot{V} c_p} \left[1 - \exp \left(- \frac{1}{\rho \dot{V} c_p R_{tot}} \right) \right]^{-1} \quad (13)$$

Eq. (13) can be simplified by using an equivalent thermal resistance R' with the temperature difference between the conductor hot spot and the coolant inlet, taking into account the temperature rise of the coolant, which leads to Eq. (14).

$$\dot{Q}_c = \frac{T_c - T_{f,i}}{R'} \quad (14)$$

The equivalent resistance is then defined by combining Eq. (13) and Eq. (14) to result in Eq. (15).

$$R' = \frac{1}{\rho \dot{V} c_p} \left[1 - \exp\left(-\frac{1}{\rho \dot{V} c_p R_{tot}}\right) \right]^{-1} \quad (15)$$

Pressure drop

Although the heat transfer coefficient is independent of the flow rate, due to the heating of the coolant, the winding temperature will be a function of the coolant flow rate. The coolant flow rate is limited by the pressure drop, which must be sufficiently low to assure that a standard pump will be able to provide the desired flow rate. The pressure drop of the flow through the winding can be estimated by determining the pressure drop Δp of a straight channel as in Eq. (16).

$$\Delta p = \frac{\rho u^2}{2} f \frac{L}{D_h} \quad (16)$$

In Eq. (16), u is the average velocity, f is the Darcy friction factor and L is the length of the channel. The length of the channel is related to the total wire length and the total number of turns (summed over the entire motor) N by Eq. (17).

$$L_{tot} = 2 N L \quad (17)$$

The total number of turns can be calculated from the wire diameter, the winding cross-sectional area S_w and the fill factor with Eq. (18).

$$N = \frac{S_w FF (D_c/D_i)^2}{2 \pi D_i^2/4} \quad (18)$$

The friction factor for fully developed laminar flow in a channel with a three-sided cusped cross section is determined by Eq. (19) [23].

$$f = \frac{26.012}{Re} = 26.012 \frac{\nu}{u D_h} \quad (19)$$

Where Re is the Reynolds number and ν is the kinematic viscosity. The pressure drop can be recalculated as in Eq. (20).

$$\Delta p = 26.012 \frac{\rho u L}{2 D_h^2} \nu \quad (20)$$

The velocity can be related to the flow rate by the total winding cross-sectional area S_w with Eq. (21).

$$u = \frac{\dot{V}}{[1-FF (D_c/D_i)^2] S_w} \quad (21)$$

Combining Eq. (20) and Eq. (21) results in Eq. (22).

$$\Delta p = C \rho(T_f) \nu(T_f) \dot{V} \quad (22)$$

The newly introduced parameter C is a constant only dependent on geometric parameters and T_f is the fluid temperature. The relation shows that the pressure drop varies linearly with the flow rate. Furthermore, the coolant density and viscosity will affect the pressure drop. The dependency of these fluid properties on the temperature is also explicitly added to the equation. Mostly the fluid viscosity is highly dependent on temperature (higher temperature results in lower viscosity) and its effect can be clearly seen in the measurements discussed in the model validation section.

Thermohydraulic model validation

Measurement setup

To validate the thermohydraulic model, an experimental setup is built of which a schematic overview is shown in Figure 4. A single concentrated winding with insulation class H is used, the characteristics of which are given in Table 2. Insulation class H indicates that the temperature of the insulation should not exceed 180 °C, making this the temperature limit for the cooling method. The wire was carefully wound to approach a perfect cylindrical packing. The winding was taped with Kapton and placed in a

milled POM housing (see picture in Figure 5 and CAD drawing in Figure 6) with silicon mastic added to seal the gaps between winding and housing. With the Kapton tape preventing the mastic from entering the gaps between the individual wires, these are kept free as flow passages.

For the tests, a 38.24% water-glycol mixture is used as coolant. This was chosen as the conditioning circuit was readily available and the thermal properties of the water-glycol mixture are accurately known. As stated previously, a dielectric fluid should be used in an actual motor to guarantee proper electrical insulation. Therefore, after the validation of the model with water-glycol as coolant, the influence of switching to a dielectric fluid, in this case automatic transmission fluid (ATF), is modeled in the following section.

A Neslab M100 chiller cools the fluid to achieve a constant inlet temperature. The coolant circuit also includes an adjustable three-way valve to vary the flow rate to the winding. Type T thermocouples measure the temperature of the fluid at the inlet and outlet. These thermocouples are calibrated by an in-house calibration procedure which results in an accuracy of ± 0.07 °C. Two pressure transducers determine the pressure at inlet and outlet, with an accuracy of respectively 0.06 bar and 0.03 bar. An oval gear flow meter measures the volumetric flow rate and has an accuracy of 1.5% of the reading value. Heat dissipation in the coil is provided by a DC source capable of delivering up to 120 A. This device also measures the current with an accuracy of 0.24 A. A Keithley 2700 multimeter determines the voltage, with a maximal error of 0.2 mV. From these two measurements, the heat dissipated in the winding and the resistance of the winding is calculated.

The measured resistance is used to determine the average temperature of the winding and to subsequently analyze the thermal performance. This can be done as the

electrical resistance varies linearly with temperature in the region of interest. The relationship between electrical resistance and temperature is determined by a calibration done beforehand. The winding is placed in an oven which is maintained at a constant temperature. A PT100 thermometer measures the temperature with an accuracy of 0.06 °C. The resistance of the winding is determined with an accuracy of 22 μΩ. This process is repeated for seven different temperature levels, ranging from 20 °C to 50 °C. A linear relation between temperature T_c and resistance R^e is determined as described by Eq. (23).

$$R^e = R_0^e [1 + \alpha(T_c - T_0)] \quad (23)$$

The reference temperature T_0 is chosen as 20 °C. The reference resistance R_0^e and temperature coefficient α are determined as 38.67 mΩ and 0.00395 1/K respectively. The temperature coefficient corresponds to values from literature for the temperature coefficient of copper at 20 °C. The linear relation is shown in Figure 7. The uncertainty on the determination of the average winding temperature from the winding resistance ranges from 0.6 °C to 1.3 °C. An overview of the sensor and derived uncertainties is given in Table 3.

57 measurement points are taken for different coolant inlet temperatures, flow rates and heat dissipation rates. A single measurement point is taken when the experimental setup achieves a steady-state condition. This is assessed by determining the standard deviation of the measured coil temperature and heat dissipation of the last 100 measurements (about four minutes). The steady-state criterion is fulfilled if the standard deviation is smaller than half of the measurement uncertainty. The maximal Reynolds of all measurement points is 183. As this is significantly smaller than 2300, the assumption of laminar flow in the channels was valid [21].

Two inputs are unknown for the model: the fill factor of the winding and the wire deformation parameter. These two values are fitted to the 57 measurement points, which results in a fill factor of 82.7% and a wire deformation parameter of 0.236. These values can also be determined with reasonable accuracy with less measurement points. When using only 10 points, the fitting procedure results in a fill factor of 82.3% and a deformation parameter of 0.225.

Hydraulic Model Validation

To validate the hydraulic model, the pressure drop is measured for flow rates varying from 0 to 1.2 l/min without any heat dissipation in the winding. The coolant temperature is varied in four levels (5 °C, 10 °C, 15 °C, 20 °C), as this will influence the viscosity of the coolant, which will in turn influence the pressure drop. The results of the measurements and modeling are shown in Figure 8. There is a clear linear relation between flow rate and pressure drop. Furthermore, the effect of temperature (and thus viscosity) changes is captured correctly. All measurement points (including those with heat dissipation) are shown in Figure 9, also indicating the measurement uncertainty of the pressure transducers with the error bars. The modeling determines the pressure drop within the measurement accuracy for all measurement points. For all used flow rates, the pressure drop remains below 1.1 bar, which is an acceptable range for drive train cooling applications.

Thermal Model Validation

Measurements with heat dissipation in the winding are performed to validate the thermal modeling. The heat dissipation (and current density) is varied in three steps: 100 W (17.9 A/mm²), 300 W (30.6 A/mm²) and 600 W (42.3 A/mm²), with the current density j defined as a function of the current I by Eq. (24).

$$j = \frac{I}{\pi D_c^2/4} \quad (24)$$

The last step has some variation in heat dissipation around 600 W, as the source was set to the maximal current (120 A), while the resistance of the winding varied with temperature from 41.4 Ω to 43.6 Ω . The inlet temperature of the coolant is set to 20 °C while the flow rate is varied between 0 and 1.5 l/min. A comparison between the measured and modeled winding temperature is shown in Figure 10. The measurements and model follow the same trend with respect to both flow rate and heat dissipation. At high flow rates, the model tends to overestimate the winding temperature. This is related to the conservative assumption of fully developed flow as explained in the thermohydraulic model section. The thermal development length, where heat transfer coefficients are higher than those in the fully developed region, is dependent on the Reynolds number and thus on the flow rate. At lower flow rates, the largest part of the channels in the winding will be subject to fully developed flow as is assumed in the modelling. At higher flow rates, a larger part of the channels in the winding will be subject to thermally developing flow, which results in lower thermal resistances in the measurements than estimated by the model. In Figure 11, the modeled winding temperature is plotted as a function of the measured winding temperature (with error bars indicating the measurement uncertainty) for all measurements with heat dissipation in the winding. The model predicts the temperature within 3 °C for all points, with the highest deviations occurring at high flow rates. The maximal absolute deviation of 3 °C can be made relative by relating it to the difference between the winding and coolant inlet temperature. This results in a relative discrepancy of 12% at the point of maximal absolute deviation. At the highest current density (42.3 A/mm²) and the highest flow rate, the pressure drop is around 1 bar and the temperature in the winding is 38.2 °C.

Performance with water-glycol as coolant

The three thermal resistances (conduction in copper, conduction through insulation and convection in the fluid) are shown in Table 4. They are shown for both water-glycol and oil as coolant, which will be discussed in the next section. The convective thermal resistance is clearly the dominant resistance, while the resistance due to conduction in the conductor is negligible due to the high thermal conductivity of the copper.

Furthermore, from Figure 12, it is clear that the sensible heating of the fluid from inlet to outlet also has a significant contribution to the overall temperature difference between fluid inlet and winding for the flow rates applied in the experiments. This figure shows the outlet and winding temperatures for a heat dissipation rate of 300 W. At lower flow rates, the coolant outlet temperature increases and becomes the dominant factor determining the winding temperature.

As the maximal temperature measured in the experiments is far below 180 °C, which is the allowable maximal temperature for wires with insulation class H, it indicates that even higher current densities are feasible with this cooling technique. Using the validated model, the variation of the conductor temperature with the current density for a pressure drop of 1 bar is simulated and shown in Figure 13. The current density can be increased to 75 A/mm² for a winding temperature of 100 °C (in practice, the current density should be limited to a slightly lower value to avoid that the coolant starts boiling). As the model overestimates the winding temperature at the flow rates corresponding to a pressure drop of 1 bar, extrapolation of the measurement leads to an even slightly higher attainable current density.

Modeled performance with oil

Oil Fluid Properties

To reduce the risk of short-circuits in the motor, it is preferred not to use water-glycol as coolant and instead use an electrically non-conductive oil. Furthermore, in an electric vehicle cooling system, the coolant temperature is typically around 65 °C so there is a large enough temperature difference with the ambient for the driving force of heat transfer in the radiator. With the validated model, an analysis can be done on the performance of the cooling method with oil at 65°C inlet temperature as coolant, in this case ATF. The fluid properties of the ATF used in the simulations are shown in Table 5 and can be compared to those of the water-glycol mixture. The fluid properties of the oil are worse for heat transfer than those of water-glycol mixtures. The lower thermal conductivity results in a higher thermal resistance, the lower density and specific heat capacity result in a higher fluid outlet temperature and the increased viscosity results in a higher pressure drop for the same flow rate. An advantage of using oil as coolant is that the boiling point of oils can be higher, therefore higher temperatures of the coolant are permissible.

Hydraulic Performance

The modeled pressure drop as a function of volumetric flow rate is shown in Figure 14 for both water-glycol at 20 °C and ATF at 65 °C as coolant. Due to the increase of the fluid viscosity, the pressure drop increases by a factor 5 for the same volumetric flow rate. This will have an impact on the outlet temperature and thus also on the winding temperature. The flow rate at a pressure drop of 1 bar is 0.28 l/min for ATF.

Thermal Performance

Due to the lower thermal conductivity of the ATF, the convective thermal resistance in the fluid R_f increases from 22.89×10^{-3} K/W for water-glycol to 67.46×10^{-3} K/W for ATF as shown in Table 4 (the conductive resistances do not change when using a different coolant). The modeled outlet and winding temperature are shown in Figure 15. Next to the convective thermal resistance, also the fluid outlet temperature changes. With oil as coolant, the winding temperature is mostly limited by the outlet temperature, while the temperature difference due to the thermal resistances (of conduction and convection) has a smaller influence. For a pressure drop of 1 bar (and the resulting flow rate of 0.28 l/min), the temperature difference between inlet and outlet is equal to 36.3 °C and the total temperature difference between fluid inlet and winding is equal to 43.6 °C. The biggest gain to be made is thus in increasing the flow rate by allowing a larger pressure drop or by choosing an oil with a lower viscosity. The flow rate is also dependent on the characteristics of the winding. For windings with a lower fill factor, the flow cross-sectional area will be larger and therefore the flow resistance lower, resulting in a higher achievable flow rate for the same pressure drop.

The feasible current densities with ATF as coolant are significantly lower compared to using water-glycol as coolant, even considering that the temperature of the winding can go up to higher values. The average winding temperature for a pressure drop of 1 bar as a function of current density is plotted in Figure 16. The maximal current density at a winding temperature of 180 °C is equal to 39.4 A/mm². This compares favorably to the other cooling techniques on standard winding topologies summarized in Table 1. The current density can be 2.6 times higher than that of a machine with water jacket cooling and can be 41% higher than the current density for

spray end winding cooling, which is the best performing cooling method apart from the direct casted coils with liquid channels.

Conclusion

Mid-conductor winding cooling is presented as a novel implementation of direct through-slot winding cooling of electric machines. This method consists of forcing a coolant flow through empty spaces in between the individual winding wires. This eliminates any thermal interface resistances and exhibits high heat transfer areas and convective heat transfer coefficients, resulting in highly effective cooling.

A thermohydraulic model of the cooling method is made and validated.

Experiments are performed on a setup with a water-glycol mixture as coolant, where the pressure drop and winding temperature are monitored. The measurements show a good correspondence with the model. The pressure drop is predicted within the measurement uncertainty (0.07 bar) and the measured winding temperatures match the modeled temperatures within 3 °C for all measurement points.

Using the validated model, the performance of the cooling technique is evaluated when using oil as coolant, which is more commonly used for direct cooling methods to avoid short-circuiting the winding. Although the heat transfer characteristics of oil are significantly inferior to those of water-glycol mixtures, the model shows that using oil is also feasible. When using oils, higher temperatures are possible in the winding and the maximal attainable current density is equal to 39.4 A/mm².

Nomenclature

A	Heat transfer area	m ²
$A_{perfect}$	Heat transfer area for perfect packing	m ²

c_p	Fluid specific heat capacity	J/kgK
C	Constant dependent on the winding geometry	1/m ³
D_c	Conductor diameter	m
D_h	Hydraulic diameter	m
D_i	Wire diameter	m
f	Darcy friction factor	-
FF	Winding fill factor	-
h	Convective heat transfer coefficient	W/m ² K
I	Current	A
j	Current density	A/m ²
k_c	Conductor thermal conductivity	W/mK
k_f	Fluid thermal conductivity	W/mK
k_i	Insulation thermal conductivity	W/mK
L	Flow length	m
L_{tot}	Wire length	m
$LMTD$	Logarithmic mean temperature difference	K
N	Number of turns	-
Nu	Nusselt number	-
p	Pressure	Pa
P	Channel perimeter	m
\dot{Q}_c	Copper losses	W
r	Radius	m
R^e	Electrical resistance	Ω
R^{e_0}	Reference electrical resistance	Ω
R'	Equivalent thermal resistance taking into account fluid heating	K/W

R_c	Conductive thermal resistance of conductor	K/W
R_f	Convective thermal resistance of fluid	K/W
R_i	Conductive thermal resistance of insulation	K/W
R_{tot}	Total thermal resistance (sum of R_c , R_i and R_f)	K/W
Re	Reynolds number	-
S	Cross-sectional channel area	m ²
S_w	Winding cross-sectional area	m ²
T	Temperature	K
T_0	Reference temperature	K
T_b	Boundary temperature	K
T_c	Conductor temperature	K
T_f	Fluid temperature	K
$T_{f,i}$	Fluid inlet temperature	K
$T_{f,o}$	Fluid outlet temperature	K
u	Average flow velocity	m/s
\dot{V}	Volumetric flow rate	m ³ /s
α	Temperature coefficient	1/K
ε	Wire deformation parameter	-
ρ	Fluid density	kg/m ³
ν	Fluid kinematic viscosity	m ² /s

Declaration of interest statement

The authors report there are no competing interests to declare.

Acknowledgements

This work was supported in part by Flanders Make, the strategic research centre for the manufacturing industry.

References

- [1] A. Tikadar, D. Johnston, N. Kumar, Y. Joshi, and S. Kumar, “Comparison of electro-thermal performance of advanced cooling techniques for electric vehicle motors,” *Appl. Therm. Eng.*, vol. 183, p. 116182, Jan. 2021, doi: 10.1016/j.applthermaleng.2020.116182.
- [2] C. Tighe, C. Gerada, and S. Pickering, “Assessment of cooling methods for increased power density in electrical machines,” in *2016 XXII International Conference on Electrical Machines (ICEM)*, Sep. 2016, pp. 2626–2632. doi: 10.1109/ICELMACH.2016.7732892.
- [3] D. Staton, A. Boglietti, and A. Cavagnino, “Solving the more difficult aspects of electric motor thermal analysis in small and medium size industrial induction motors,” *IEEE Trans. Energy Convers.*, vol. 20, no. 3, pp. 620–628, Sep. 2005, doi: 10.1109/TEC.2005.847979.
- [4] M. K. Yoon and S. Ken Kauh, “Thermal Analysis of a Small, Totally Enclosed, Fan-Cooled Induction Motor,” *Heat Transf. Eng.*, vol. 26, no. 4, pp. 077–086, May 2005, doi: 10.1080/01457630590916310.
- [5] M. Cavazzuti, G. Gaspari, S. Pasquale, and E. Stalio, “Thermal management of a Formula E electric motor: Analysis and optimization,” *Appl. Therm. Eng.*, vol. 157, p. 113733, Jul. 2019, doi: 10.1016/j.applthermaleng.2019.113733.
- [6] Z. Liu, T. Winter, and M. Schier, “Direct Coil Cooling of a High Performance Switched Reluctance Machine (SRM) for EV/HEV Applications,” *SAE Int. J. Altern. Powertrains*, vol. 4, no. 1, pp. 162–169, 2015.

[7] M. Popescu, D. A. Staton, A. Boglietti, A. Cavagnino, D. Hawkins, and J. Goss, “Modern Heat Extraction Systems for Power Traction Machines—A Review,” *IEEE Trans. Ind. Appl.*, vol. 52, no. 3, pp. 2167–2175, May 2016, doi: 10.1109/TIA.2016.2518132.

[8] J. Pyrhönen, P. Lindh, M. Polikarpova, E. Kurvinen, and V. Naumanen, “Heat-transfer improvements in an axial-flux permanent-magnet synchronous machine,” *Appl. Therm. Eng.*, vol. 76, pp. 245–251, Feb. 2015, doi: 10.1016/j.applthermaleng.2014.11.003.

[9] Y. Sun, S. Zhang, G. Chen, Y. Tang, and F. Liang, “Experimental and numerical investigation on a novel heat pipe based cooling strategy for permanent magnet synchronous motors,” *Appl. Therm. Eng.*, vol. 170, p. 114970, Apr. 2020, doi: 10.1016/j.applthermaleng.2020.114970.

[10] H. Vansompe and P. Sergeant, “Extended End-Winding Cooling Insert for High Power Density Electric Machines With Concentrated Windings,” *IEEE Trans. Energy Convers.*, vol. 35, no. 2, pp. 948–955, Jun. 2020, doi: 10.1109/TEC.2019.2953577.

[11] V. Madonna, P. Giangrande, A. Walker, and M. Galea, “On the Effects of Advanced End-Winding Cooling on the Design and Performance of Electrical Machines,” in *2018 XIII International Conference on Electrical Machines (ICEM)*, Sep. 2018, pp. 311–317. doi: 10.1109/ICELMACH.2018.8507170.

[12] T. Davin, J. Pellé, S. Harmand, and R. Yu, “Experimental study of oil cooling systems for electric motors,” *Appl. Therm. Eng.*, vol. 75, pp. 1–13, Jan. 2015, doi: 10.1016/j.applthermaleng.2014.10.060.

- [13] M. H. Park and S. C. Kim, "Thermal characteristics and effects of oil spray cooling on in-wheel motors in electric vehicles," *Appl. Therm. Eng.*, vol. 152, pp. 582–593, Apr. 2019, doi: 10.1016/j.applthermaleng.2019.02.119.
- [14] R. S. Bartle, K. Menon, and E. Walsh, "Pool boiling of resin-impregnated motor windings geometry," *Appl. Therm. Eng.*, vol. 130, pp. 854–864, Feb. 2018, doi: 10.1016/j.applthermaleng.2017.11.053.
- [15] M. Schiefer and M. Doppelbauer, "Indirect slot cooling for high-power-density machines with concentrated winding," in *2015 IEEE International Electric Machines & Drives Conference (IEMDC)*, May 2015, pp. 1820–1825. doi: 10.1109/IEMDC.2015.7409311.
- [16] N. A. Rahman, E. Bostanci, and B. Fahimi, "Thermal analysis of switched reluctance motor with direct in-winding cooling system," in *2016 IEEE Conference on Electromagnetic Field Computation (CEFC)*, Nov. 2016, pp. 1–1. doi: 10.1109/CEFC.2016.7816110.
- [17] P. M. Lindh *et al.*, "Direct Liquid Cooling in Low-Power Electrical Machines: Proof-of-Concept," *IEEE Trans. Energy Convers.*, vol. 31, no. 4, pp. 1257–1266, Dec. 2016, doi: 10.1109/TEC.2016.2597059.
- [18] C. Wohlers, P. Juris, S. Kabelac, and B. Ponick, "Design and direct liquid cooling of tooth-coil windings," *Electr. Eng.*, vol. 100, no. 4, pp. 2299–2308, Dec. 2018, doi: 10.1007/s00202-018-0704-x.
- [19] J. F. Gieras, *Advancements in electric machines*. Dordrecht: Springer, 2008.
- [20] W. A. Peterson and A. P. Lyons, "Stator construction for high performance rotating machines," 6787948 B2, Sep. 07, 2004 Accessed: Jul. 13, 2021. [Online]. Available: <https://patents.justia.com/patent/6787948>

[21] I. T’Jollyn, J. Nonneman, and M. D. Paepe, “Thermohydraulic Modelling of Microchannel Winding Cooling for Electric Machines,” in *2020 International Conference on Electrical Machines (ICEM)*, Aug. 2020, vol. 1, pp. 1004–1010. doi: 10.1109/ICEM49940.2020.9270729.

[22] I. T’Jollyn, J. Nonneman, and M. De Paepe, “Thermally developing laminar flow and heat transfer characteristics in a three-sided cusped duct,” in *Proceedings of the 15th International Conference on Heat Transfer, Fluid Mechanics and Thermodynamics (HEFAT2021)*, 2021, pp. 2234–2238. Accessed: Jul. 27, 2022. [Online]. Available: <http://hdl.handle.net/1854/LU-8718039>

[23] R. K. Shah and A. L. London, *Laminar flow forced convection in ducts: a source book for compact heat exchanger analytical data*. New York: Academic Press, 1978.

Tables

Table 1. Current density for selected cooling techniques.

Cooling technique	j [A/mm²]
Air cooled [19]	5 - 8
Water or oil jacket [19]	10 - 15
Tube end winding cooling [11]	11.97
Direct contact water jacket [10]	19.0
Indirect slot cooling [15]	20
Conductive end winding insert [10]	26.5
Spray end winding cooling [19]	28
Casted coil with liquid channels [18]	100

Table 2. Characteristics of winding used in experiments.

Conductor diameter	D_c	1.9 mm
Conductor thermal conductivity	k_c	385 W/mK
Wire diameter	D_i	2 mm
Insulation thermal conductivity	k_i	0.26 W/mK
Flow length	L	122 mm
Number of turns	N	26

Table 3. Uncertainty of measured and derived quantities.

Quantity	Uncertainty
Inlet pressure	± 0.06 bar
Outlet pressure	± 0.03 bar
Volumetric flow rate	$\pm 1.5\%$
Current	± 0.24 A
Voltage	± 0.2 mV
Fluid temperature	± 0.07 °C
Average winding temperature	$\pm 0.6 .. 1.3$ °C

Table 4. Thermal resistances of the conductor, insulation and fluid for water-glycol and ATF as coolant.

	R_c [K/W]	R_i [K/W]	R_f [K/W]
Water-glycol (20 °C)	0.0375e-3	5.696e-3	22.89e-3
ATF (65 °C)	0.0375e-3	5.696e-3	67.46e-3

Table 5. Water-glycol (38.24%) mixture properties at 20 °C and ATF properties at 65 °C.

	k_f [W/mK]	ρ [kg/m ³]	c_p [J/kgK]	ν [m ² /s]
Water-glycol (20 °C)	0.43	1050	3555	$2.564 \cdot 10^{-6}$
ATF (65 °C)	0.16	838	2112	$16.01 \cdot 10^{-6}$

List of figures

Figure 1. Mid-conductor winding cooling, arrows indicate coolant flow.

Figure 2. Conceptual design of a six-pole stator with concentrated windings and mid-conductor winding cooling. Top: 3D CAD view. Bottom: 2D cross-sectional view.

Figure 3. Perfectly packed circular wires without (left) and with deformation (right).

Figure 4. Schematic overview of the experimental setup.

Figure 5. Experimental setup: winding and housing.

Figure 6. Experimental setup: CAD drawing of winding and housing, showing flow inlet and outlet and pressure sensors.

Figure 7. Calibration curve for winding resistance as function of temperature.

Figure 8. Measured (marker) and modeled (solid line) pressure drop as a function of flow rate for different coolant temperatures.

Figure 9. Modeled pressure drop as a function of measured pressure drop.

Figure 10. Measured (marker) and modeled (solid line) winding temperature as a function of flow rate for different heat dissipation rates.

Figure 11. Modeled winding temperature as a function of measured winding temperature.

Figure 12. Measured and modeled outlet and winding temperature as a function of flow rate for 300 W winding heat dissipation.

Figure 13. Measured and modeled winding temperature as a function of current density for a pressure drop equal to 1 bar.

Figure 14. Pressure drop as a function of volumetric flow rate for water-glycol and ATF as coolant.

Figure 15. Modeled outlet and winding temperature as a function of ATF flow rate for a winding heat dissipation rate of 300 W.

Figure 16. Modeled winding temperature as a function of current density for a pressure drop of 1 bar with ATF as coolant.

Figures

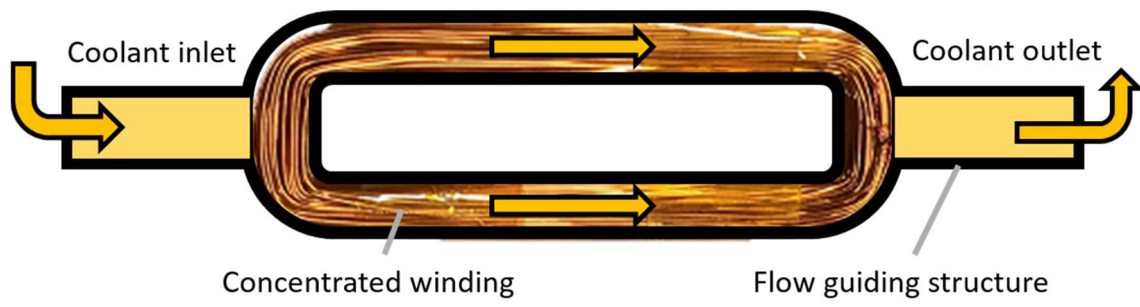


Figure 1. Mid-conductor winding cooling, arrows indicate coolant flow.

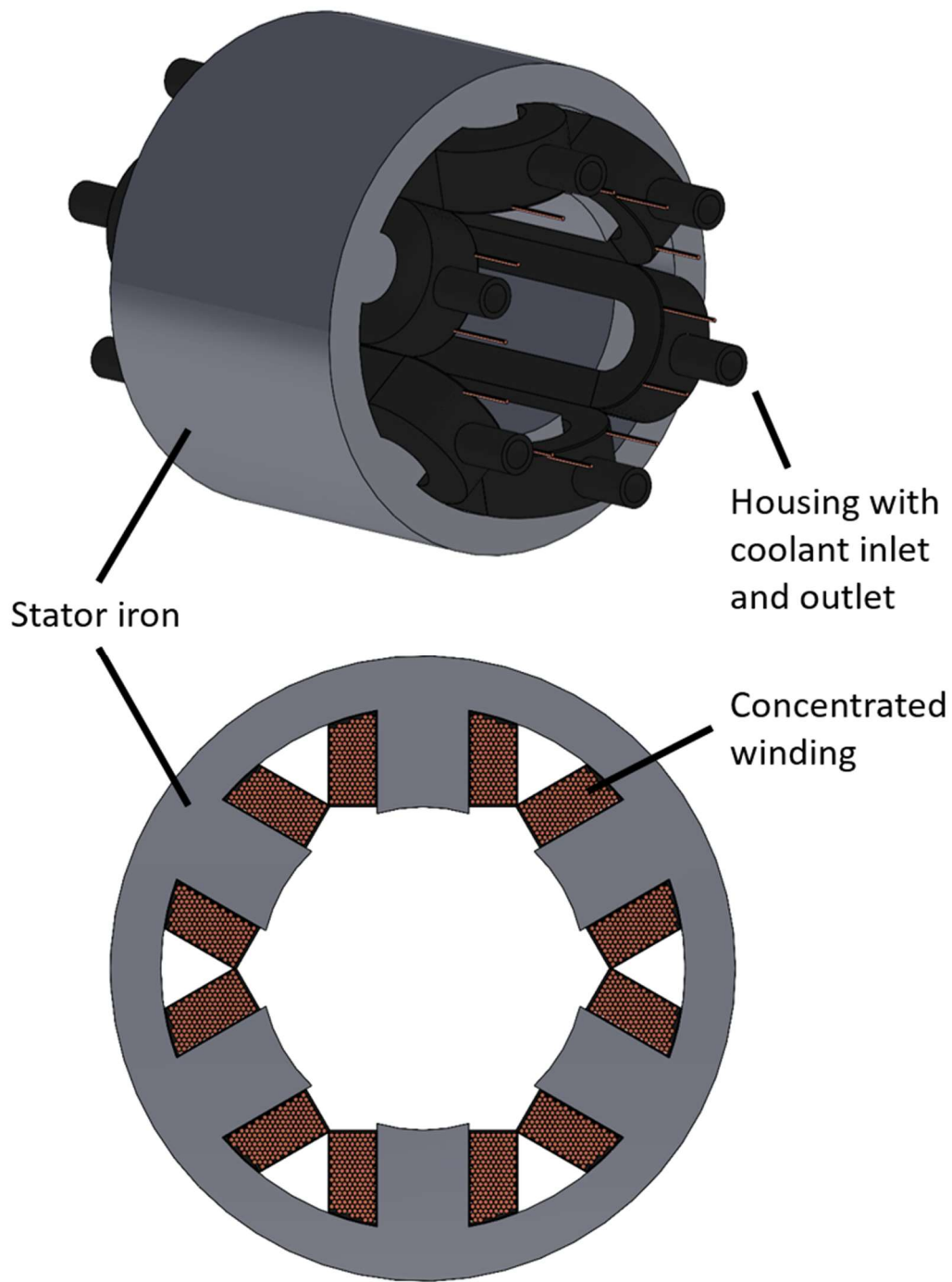


Figure 2. Conceptual design of a six-pole stator with concentrated windings and mid-conductor winding cooling. Top: 3D CAD view. Bottom: 2D cross-sectional view.

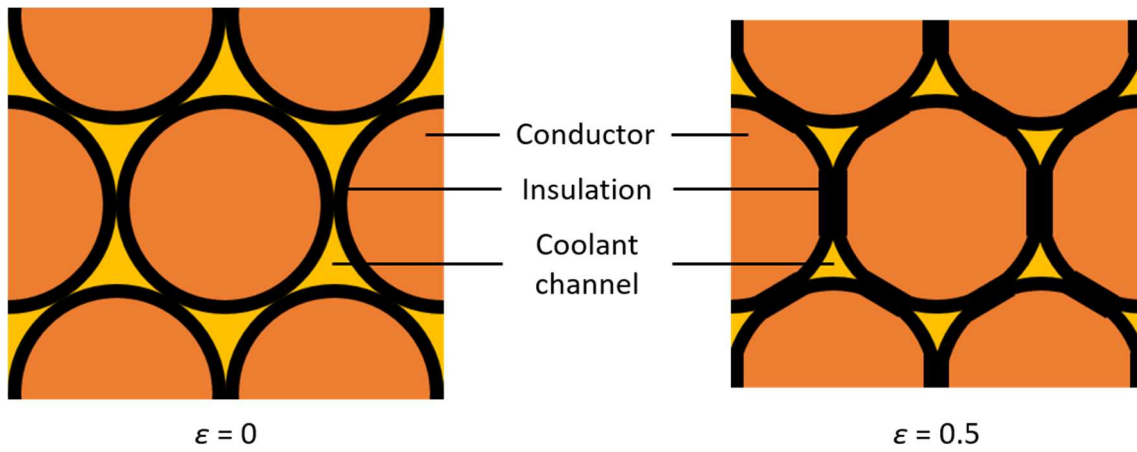


Figure 3. Perfectly packed circular wires without (left) and with deformation (right).

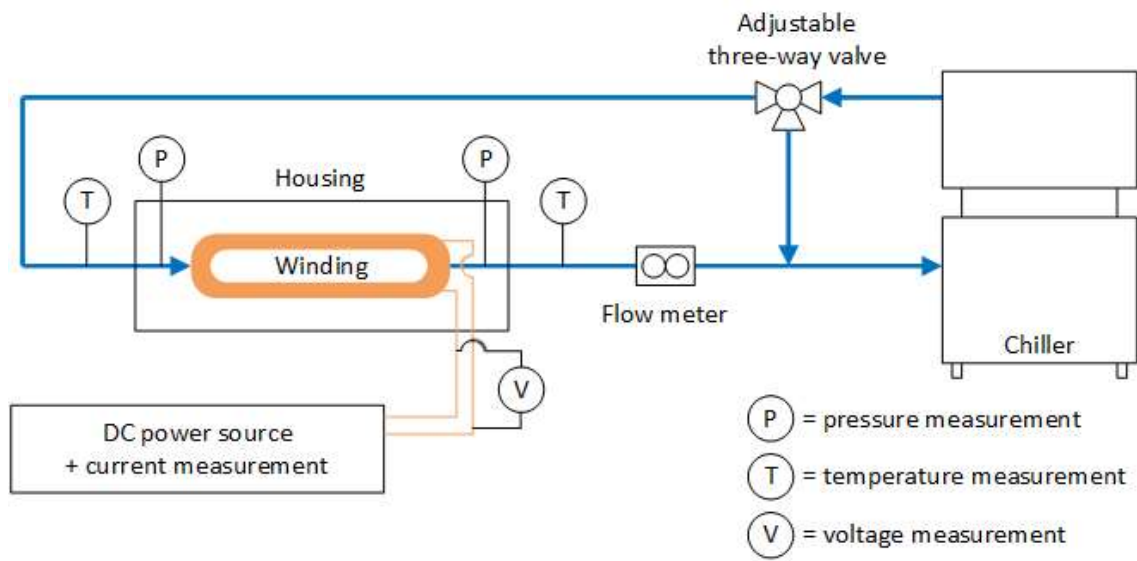


Figure 4. Schematic overview of the experimental setup.



Figure 5. Experimental setup: winding and housing.

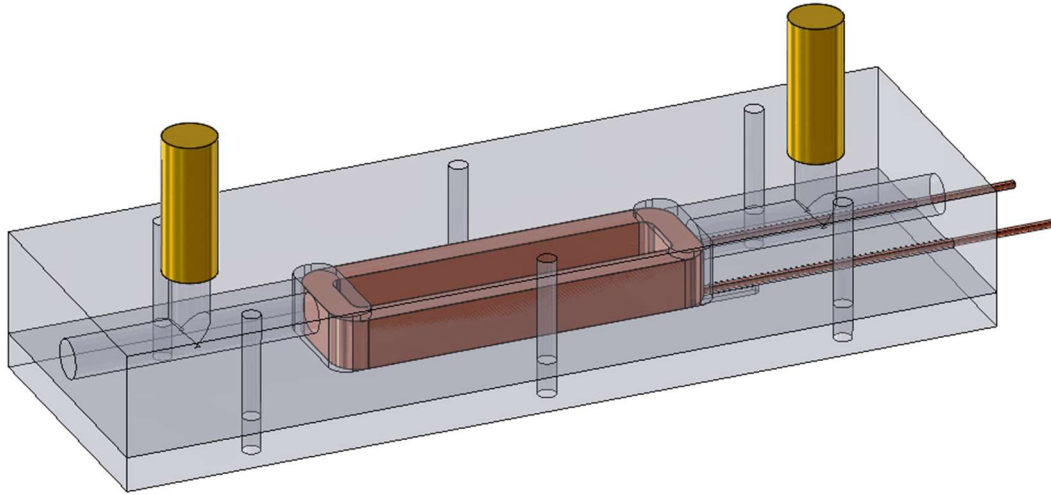


Figure 6. Experimental setup: CAD drawing of winding and housing, showing flow inlet and outlet and pressure sensors.

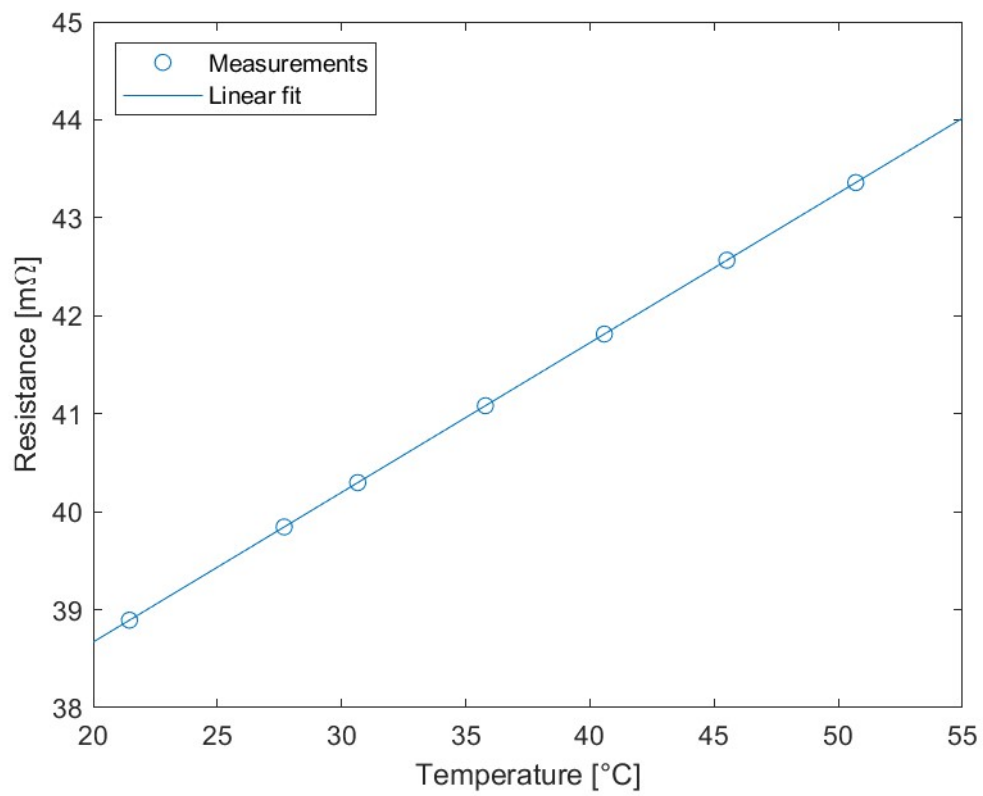


Figure 7. Calibration curve for winding resistance as function of temperature.

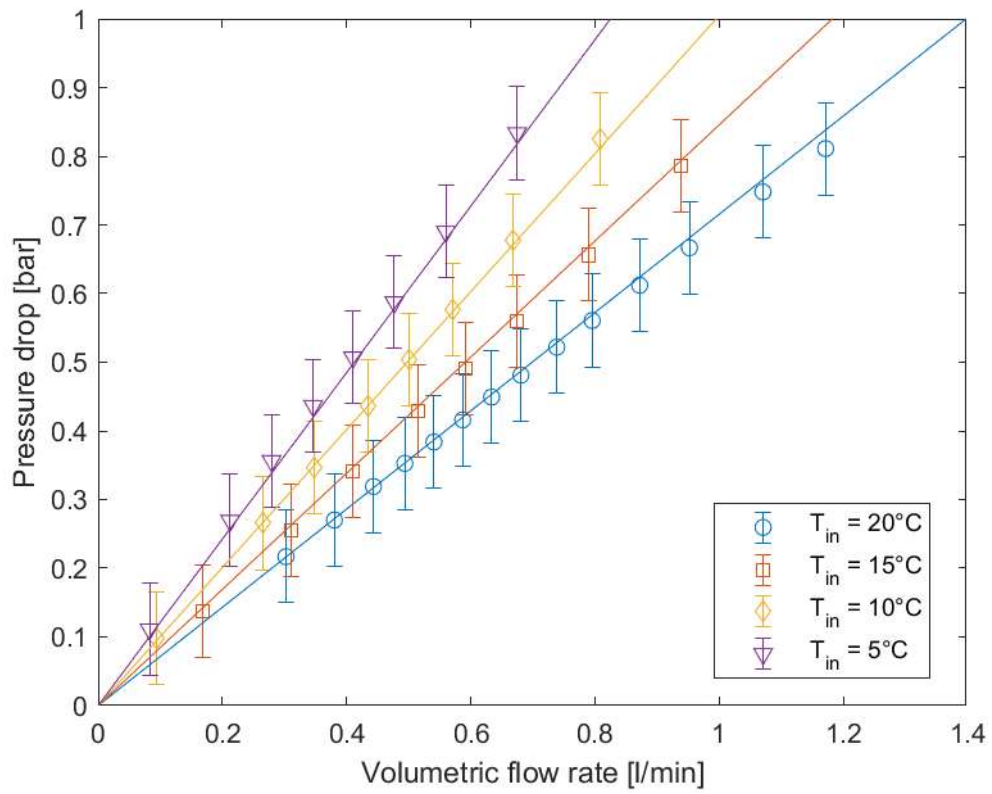


Figure 8. Measured (marker) and modeled (solid line) pressure drop as a function of flow rate for different coolant temperatures.

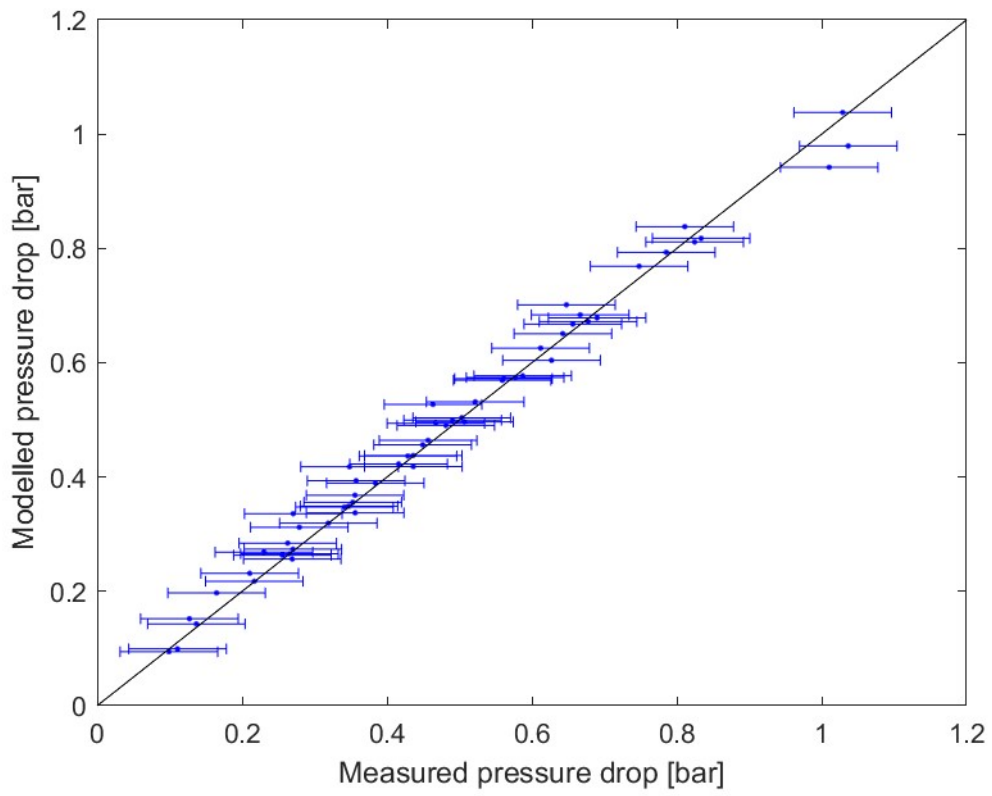


Figure 9. Modeled pressure drop as a function of measured pressure drop.

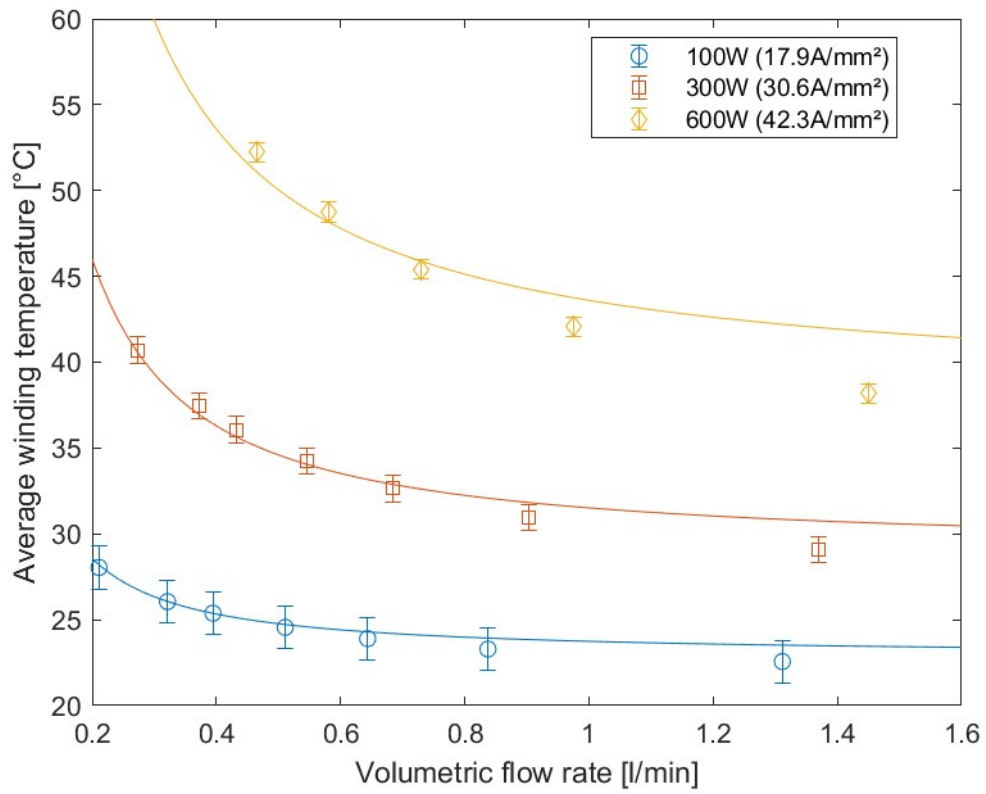


Figure 10. Measured (marker) and modeled (solid line) winding temperature as a function of flow rate for different heat dissipation rates.

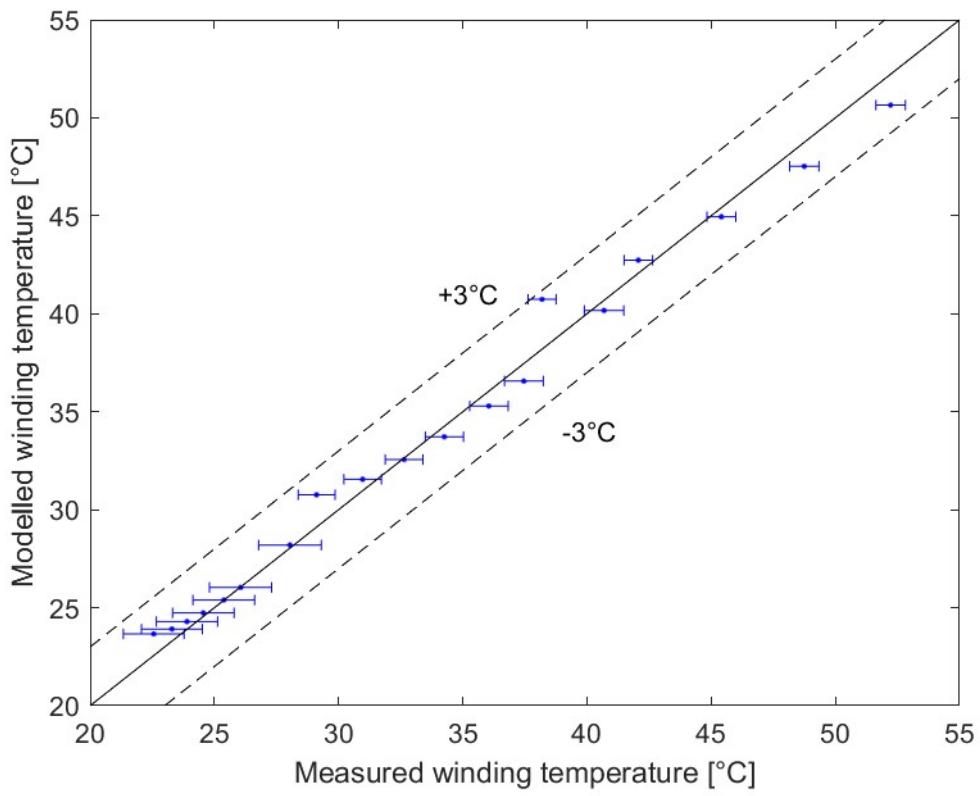


Figure 11. Modeled winding temperature as a function of measured winding temperature.

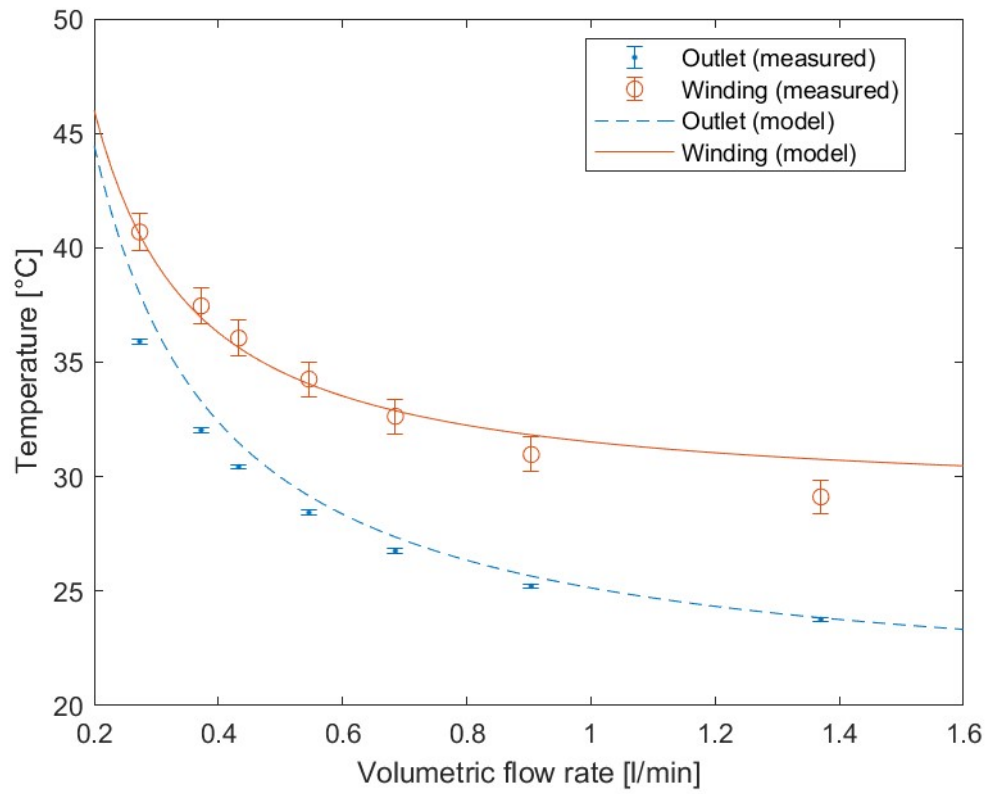


Figure 12. Measured and modeled outlet and winding temperature as a function of flow rate for 300 W winding heat dissipation.

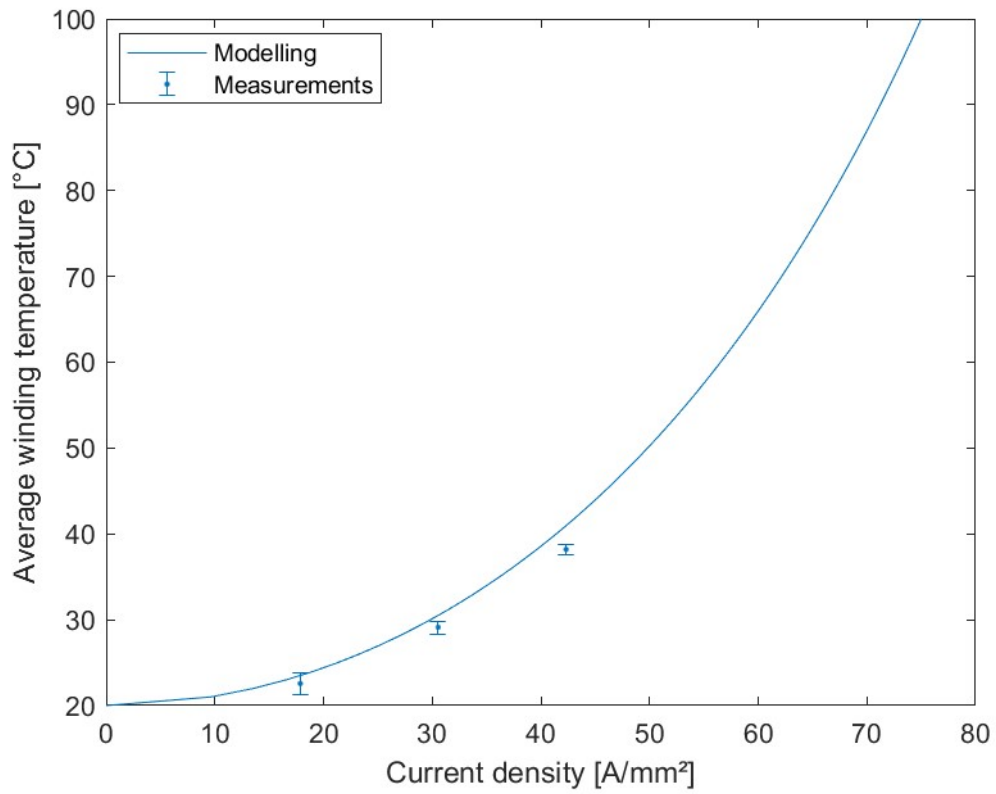


Figure 13. Measured and modeled winding temperature as a function of current density for a pressure drop equal to 1 bar.

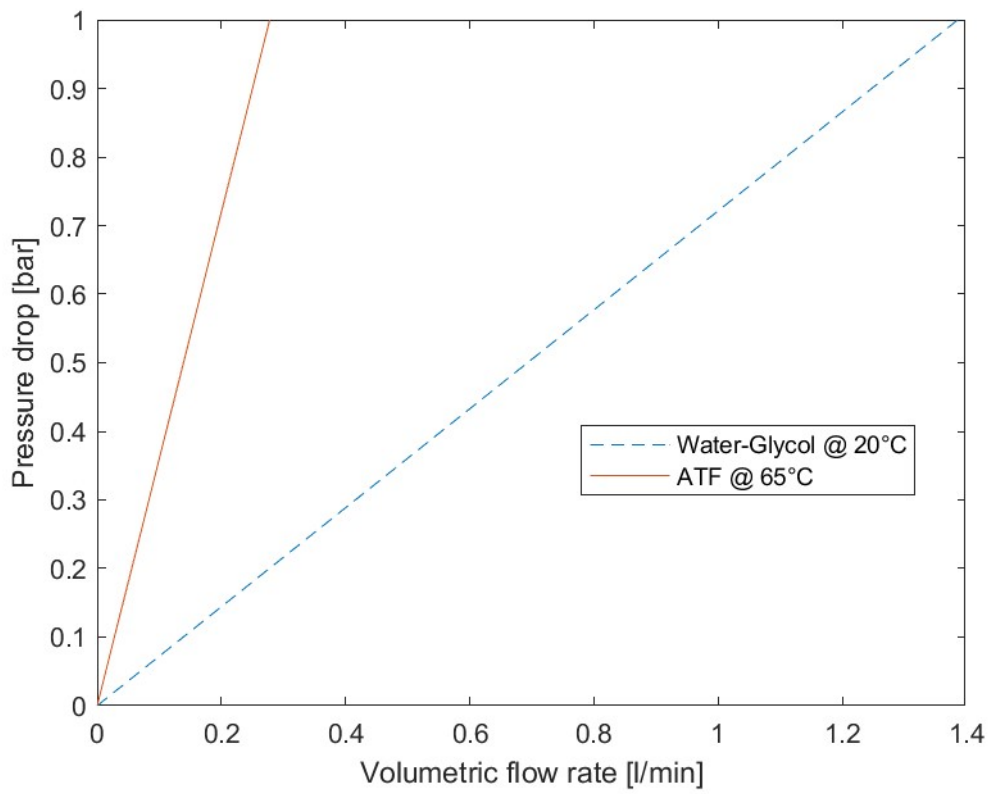


Figure 14. Pressure drop as a function of volumetric flow rate for water-glycol and ATF as coolant.

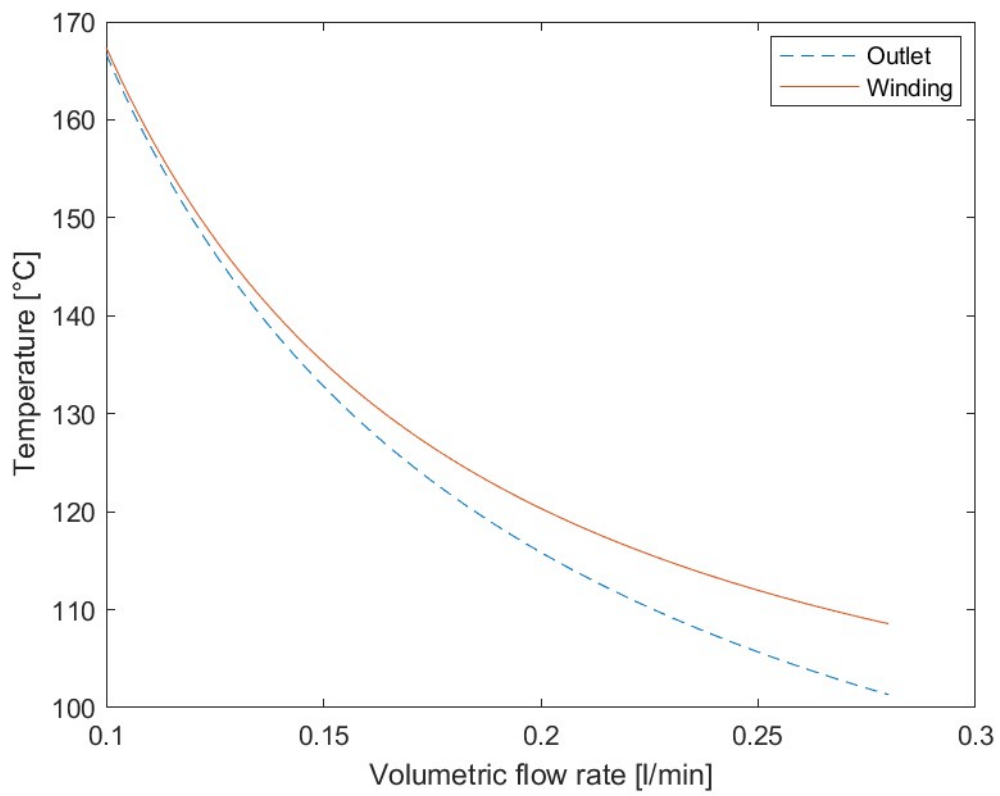


Figure 15. Modeled outlet and winding temperature as a function of ATF flow rate for a winding heat dissipation rate of 300 W.

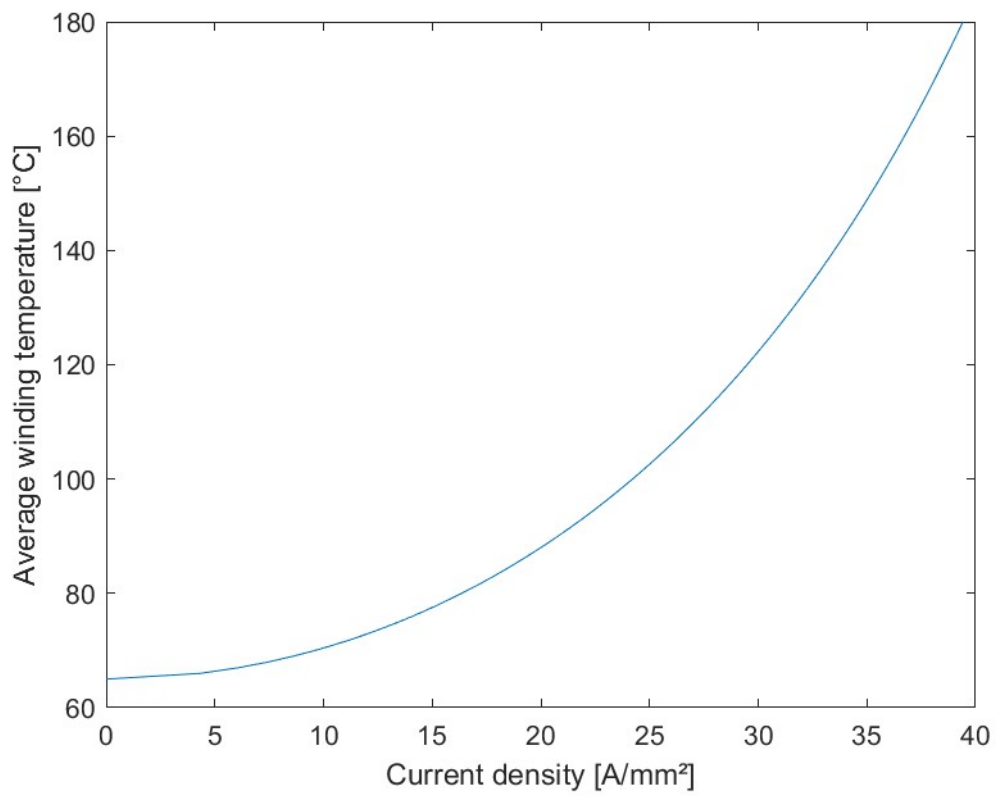


Figure 16. Modeled winding temperature as a function of current density for a pressure drop of 1 bar with ATF as coolant.

Biographies



Ilya T'Jollyn (°1992) received his M.Sc. degree in Electromechanical Engineering from Ghent University, Ghent, Belgium in 2014. In 2021, he successfully defended his doctoral dissertation with the title ‘Assessment of Nucleate Pool Boiling Heat Transfer and Critical Heat Flux for Power Electronics Cooling with a Low-GWP Refrigerant’. He is currently a postdoctoral researcher in the research group

Sustainable Thermo-Fluid Energy Systems of the Department of Electromechanical, Systems and Metal Engineering at Ghent University. His research interests include heat transfer in electrical machines and systems and he is currently working on two-phase power electronics cooling and innovative motor cooling techniques.



Jasper Nonneman (°1993) received his B.Sc. degree Electromechanical Engineering in 2014 and M.Sc. degree Mechanical Energy Engineering 2016, both from the Faculty of Engineering and Architecture, Ghent University, Belgium. He is currently working as a PhD researcher at the research group Sustainable Thermo-Fluid Energy Systems of the Department of Electromechanical, Systems and Metal Engineering at

Ghent University, Belgium. His research interests are the cooling and thermal modeling of electric machines and power electronics.



Michel De Paepe (°1972) is professor of Thermodynamics and Heat Transfer at the Faculty of Engineering and Architecture of the Ghent University. He graduated as M.Sc. in Electromechanical Engineering at the Ghent University in 1995. In 1999 he obtained the PhD in Electromechanical Engineering at the Ghent University, graduating on 'Steam Injected Gas Turbines with water Recovery'. Michel De Paepe

is currently part of the Research Group Sustainable Thermo-Fluid Energy Systems at the Faculty of Engineering and Architecture of the Ghent University. Research in this group focuses on: thermodynamics of new energy systems, performance of HVAC systems and energy in buildings and complex heat transfer phenomena in industrial applications, as in compact heat exchangers, combustion engines, electrical drives, refrigerant two-phase flow and electronics cooling. Michel De Paepe was supervisor/promotor of 29 PhDs defended at Ghent University. He is (co)author of 130 papers published in international peer reviewed journals and more than 430 conference papers.